# 1 / Magnetic Systems and Magnetic Equivalent Circuits

The purpose of this chapter is set forth the basic background needed to analyze electromagnetic and electromechanical systems. The first step to doing this is to set forth the notion of magnetic equivalent circuit – an approximate but often fairly accurate technique for the analysis of magnetic systems. Using this technique, we will see how to translate a geometrical description of a magnetic device consisting of coils of wire, magnetic conductor such as iron, and permanent magnet material into an electrical circuit description. It should be noted that throughout this work, SI units will be strictly adhered to. Thus, flux density is measured in Tesla and field intensity in A/m. The reader is referred to [1] for a discussion of other unit systems. As an additional note, with regard to notation, vector and matrix quantities will appear in a bold, non-italicized font throughout this work. Scaler quantities will appear in a non-bold, italicized font. Thus, for quantity such a flux density, $\mathbf{B}$ refers to a flux density vector, whereas $B$ refers to a scalar representing the flux density in some particular direction (such as along a specified path)

## 1.1 MMF AND KIRCHOFF'S VOLTAGE LAW FOR MAGNETIC CIRCUITS

We begin our analysis of magnetic system by developing the concept of Kirchoff's voltage law for magnetic systems – in particular the idea that the sum of the magneto-motive force drops around any closed loop is equal to the sum of the magneto-motive force sources. To formalize this idea, we begin with Ampere's law, which states that the line integral of the field intensity is equal to the current enclosed by that path. This is illustrated in Fig. 1.1-1 and may be stated mathematically as

$$\oint_x \mathbf{H} \cdot d\mathbf{l} = i_x \tag{1.1-1}$$

In (1.1-1), $\mathbf{H}$ is the field intensity (a vector field), $d\mathbf{l}$ is an incremental segment in the path (again a vector), $x$ denotes a path, and $i_x$ is the total current enclosed by that path, where the sign is determined in accordance with the right-hand rule.

The total enclosed current for the path is the total magneto-motive force source $F_x$ for the path, i.e.

$$F_x = i_x \tag{1.1-2}$$

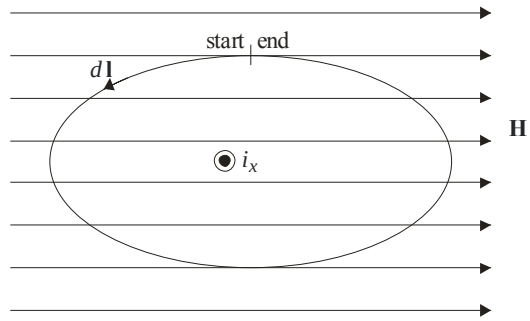

Figure 1.1-1. Illustration of Ampere's Law.

It will often be convenient to break the total enclosed current into a number of separate components, i.e.

$$i_x = \sum_{j=1}^{J} i_{x,j} \tag{1.1-3}$$

where $J$ is the number of components. Each component can be viewed as a magneto-motive force source component

$$F_{x,j} = i_{x.j} \tag{1.1-4}$$

Comparing (1.1-2)-(1.1-4)

$$F_x = \sum_{j=1}^{J} F_{x,j} \tag{1.1-5}$$

It will be also be convenient to break the path integral in (1.1-1) into a number of sub line-integrals as depicted in Fig. 1.1-2. If the path integral is broken into $K$ segments we have

$$\sum_{k=1}^{K-1} \int_{l_k}^{l_{k+1}} \mathbf{H} \cdot d\mathbf{l} + \int_{l_K}^{l_1} \mathbf{H} \cdot d\mathbf{l} = F_x \tag{1.1-6}$$

where at this point it is convenient to define a magneto-motive force drop as

$$F_{a,b} = \int_{l_a}^{l_b} \mathbf{H} \cdot d\mathbf{l} \tag{1.1-7}$$

Combining (1.1-5)-(1.1-7), we have that

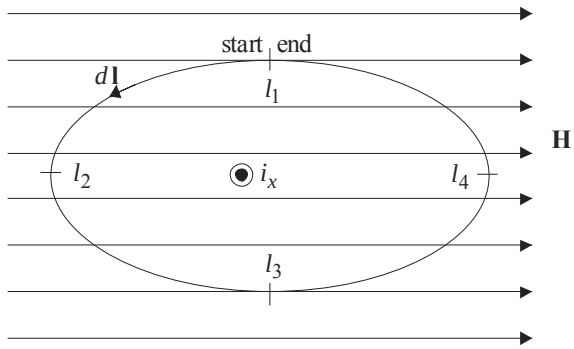

Figure 1.1-2. Division of path into sub-intervals.

$$\sum_{k=1}^{K-1} F_{k,k+1} + F_{K,1} = \sum_{j=1}^{J} F_{x,j} \tag{1.1-8}$$

This result is Kirchoff's magnetomotive force law for magnetic circuits, which may be stated as: **The sum of the MMF drops around a closed loop is equal to the sum of the MMF sources for that loop.**

## 1.2 FLUX AND KIRCHOFF'S CURRENT LAW FOR MAGNETIC CIRCUITS

For electric circuits, Kirchoff's current law states that the sum of the current into a node of an electric circuit is equal to zero. As it turns out, the same can be said of flux in a magnetic circuit. To see this, we must first define a node of the magnetic circuit, which will be taken to be a closed volume which is small enough that the MMF drop between any two points is negligible. Example nodes in a cut toroid magnetic core are illustrated in Fig. 1.2-1. This core has an inner radius $r_i$, and outer radius $r_o$, and extends a depth $d$ into the page. The core has been cut in half, and the two halves separated by a distance $g$. One possible choice of nodes is illustrated; a formal discussion of how to select nodes is set forth in Section 1.4.2. In this example, each node has dimensions $(r_0 - r_i)$ by $d$ (into the page) by $\varepsilon$ for a total volume of $(r_o - r_i)d\varepsilon$, where $\varepsilon$ is the dimension of the node in the direction of the $\mathbf{H}$ field. By letting $\varepsilon \to 0$, the MMF drop across the node is zero.

To derive Kirchoff's current law for magnetic circuits, we begin with Gausse's Law which states that the surface integral of flux density over a closed volume is zero. In particular,

$$\oint \mathbf{B} \cdot d\mathbf{S} = 0 \tag{1.2-1}$$

where $\mathbf{B}$ is flux density and $d\mathbf{S}$ in an incremental surface area.

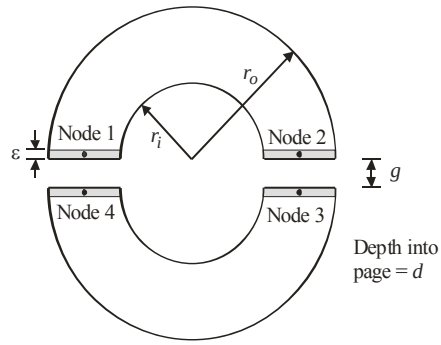


Figure 1.2-1. Nodes in a magnetic circuit.

It is convenient to break the surface integral (1.2-1) into $M$ regions where $S_m$ denotes the $m$'th region of the set. This yields

$$\sum_{m=1}^{M} \int_{S_m} \mathbf{B} \cdot d\mathbf{S} = 0 \tag{1.2-2}$$

Flux is defined as the integral of the normal component of a field over a surface. Stated mathematically, the flux through surface region $m$ may be expressed

$$\Phi_m = \int_{\mathbf{S}_m} \mathbf{B} \cdot d\mathbf{S} \tag{1.2-3}$$

Substitution of (1.2-3) into (1.2-2) yields

$$\sum_{m=1}^{M} \Phi_m = 0 \tag{1.2-4}$$

This relationship establishes Kirchoff's current law for magnetic circuits, which can be stated as: **The sum of the flux leaving a node of a magnetic circuit is zero.**

## 1.3 MATERIAL CHARACTERISTICS AND OHM'S LAW FOR MAGNETIC CIRCUITS

In both magnetic and electric circuits, Kirchoff's laws are in fact physical laws – they stem directly from Maxwell's equations. However, in electric circuits, a third commonly quoted physical law, in particular Ohm's law, is not a physical law at all but is instead a property of some types of conducting materials. The same can be said of Ohm's law for magnetic circuits; it is not a physical law, merely a property that some materials possess.

The interaction of materials with magnetic fields stems from two principal effects, the first of which arises because of the magnetic moment of the electron as it moves through it's shell (crudely viewed as the moment of the electron moving

through an orbit), and the second effect is due to the magnetic moment that arises because of electron spin. The interaction of these two effect produces six different types of materials – diamagnetic, paramagnetic, ferromagnetic, antiferromagnetic, ferrimagnetic, and superparamagnetic.

The diamagnetic effect is present in all materials, and has a net effect of acting against an applied magnetic field. Consider a electron moment caused by the electron moving within its shell. An applied field will create an outward force on the electron. However, the Coulomb force on the electron is unaffected. Since the effective radius of the electron's orbit (as viewed in crude terms) is fixed by the shell, the electron must slow, thereby reducing the moment of the electron moving in its shell. Diamagnetic materials are those materials in which the diamagnetic effect dominates other mechanisms so that the material's field tend to act against the applied field. In these materials, the net magnetic moment of the material is either zero or vary small. Diamagnetic materials include hydrogen, helium, copper, gold, and silicon.

Let us next consider paramagnetic materials. In these materials there is a small net magnetic moment. The moments due to electron spin do not quite cancel the moments of electrons within their shells. In this case, the moments will align with an applied field, which tends to aide the applied filter. Materials in which the tendancy to aid the field overcomes the diamagnetic effect are called paramagnetic. Paramagnetic materials include oxygen and tungsten.

In ferromagnetic, anti-ferromagnetic, ferromagnetic, and superparamagnetic materials, the individual atoms possess a strong net moment. In ferromagnetic materials the atoms posses a large net moment, and interatomic forces are such to cause these moments to line up over large regions called domains. In the absence of an external field, the net effect of the net moments of the domains is to cancel out; however in the presence of an external field the domain walls will move in such a way which domains which are aligned with the applied field will grow; and domains which are not aligned will shrink. This class of materials has a very strong interaction with external fields are very important in engineering applications. Materials which possess this property at room temperature include iron, nickel, and cobalt.

Anti-ferromagnetic materials posses the property that interatomic forces cause the magnetic moments of adjacent atoms to be aligned in an anti-parallel fashion. The net magnetic moment of a group of atoms is therefore zero. These materials are not greatly affected by the presence of an external field.

Ferrimagnetic materials are similar to anti-ferromagnetic materials in that the magnetic moments of adjacent atoms are aligned in an anti-parallel fashion; however in this case the moments between directions are unequal. These materials exhibit a significant response to an external field. While their response is, in generally, less than that of ferromagnetic materials, one class of ferrimagnetic materials (ferrites) have a conductivity which is much lower than ferromagnetic materials, making them very well suited for high-frequency applications. Examples of ferrites include iron oxide magnetite ($Fe_3O_4$), nickel-zink ferrite ($Ni_{1/2},Zn_{12}Fe_2O_4$), and nickel ferrite ($NiFe_2O_4$).

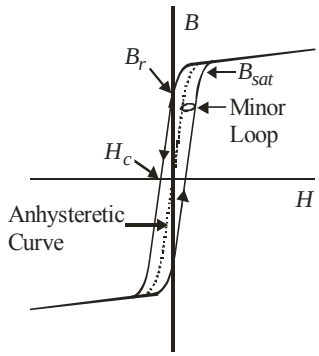


Figure 1.3-1. *B-H* characteristic of ferromagnetic and ferromagnetic materials.

A final class of materials which is useful in magnetic tape is superparamagnetic materials which consist of ferromagnetic materials in a nonferromagnetic matrix, which blocks domain wall movement.

For a more extensive discussion of the different types of materials, the reader is referred to [2]. However, our interest will primarily be in ferromagnetic and ferrimagnetic materials; other materials we will simply consider have the same response to a magnetic material as a vacuum. In both ferromagnetic and ferrimagnetic materials, the relationship between flux density $B$ and field intensity $H$ is depicted in Figure 1.3-1. As can be seen, the value of flux density $B$ cannot be uniquely established from the value of field intensity $H$ for values in the vicinity of the origin. This is because of an effect known as magnetic hysteresis which result from domain wall motion. In particular, as the domain walls move, they become 'stuck' at pinning sites which are defects in the lattice. The movement of the domain walls past the lattice requires a amount of non-recoverable energy – this loss results in hysteresis. The direction of the traversal of the loop is indicated with arrows in Figure 1.3-1. While large excitations of the core results in the complete traversal of the loop, it is also possible to enter the central region of the loop. Such a traversal is known as a minor loop. Parameters of interest that characterize the loop include the coercive force $H_c$ and residual flux density $B_r$. Hysteresis is a extremely difficult to model effect; detailed trajectories of $B$ versus $H$ are normally calculated using either a variant of the Jiles-Atherton model [3,4,5] or the Praisach-model [6]. However, even these techniques have limited accuracy. Estimates of hysteresis losses are often accomplished using the Steinmetz relationship [7], however this is only a behavioral representation.

Because of the complexity of predicting or even describing the behavior of the $B$ versus $H$ characteristic, we will largely confine our attentions to a very simple model – simply ignoring the hystereses effect. While such an approach may appear rash, it is generally the case that most of the energy storage in electromagnetic systems occurs in air – not in the magnetic material. As a result, for the majority of designs, hysteresis losses are modest.

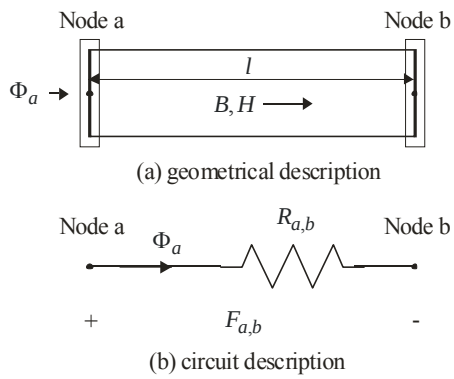


Figure 1.3-2. Segment of magnetic material.

Neglecting hystereses yields the anysteretic $B$ versus $H$ characteristic which is also shown in Figure 1.3-1. Note that even this characteristic is not trivial; after the flux density reaches a value of $B_{sat}$ the slope of the anysteretic curve decreases markedly as the material saturates. Normally, a high degree of saturation is to be avoided as it can result in large currents and high losses. In addition, the anysteretic curve is subject to an additional non-linearity at very low flux levels (not shown in Figure 1.3-1). In particular, the slope of the ahysteretic $B$ versus $H$ characteristic also drops at very low flux levels. This can be an important effect when employing parameter identification using small signal perturbations.

### 1.3.1 Linear Material

Although the relationship between flux density and field intensity can be quite complex, if the material is not saturated, and not subject to significant hysteresis, then in many anisotropic materials the relationship between flux density $\mathbf{B}$ and field intensity $\mathbf{H}$ may be expressed

$$\mathbf{B} = \mu \mathbf{H} \tag{1.3-1}$$

where $\mu$ is called the permeability of the material. Let us now consider a segment of material of length $l$ and cross sectional area $A$ in which the $B$ and $H$ fields are uniform and directed in the same direction as indicated in Fig. 1.3-2a.

Since the direction of the field has been defined, we can treat both $B$ and $H$ as scalar variables whereupon (1.3-1) reduces to

$$B = \mu H \tag{1.3-2}$$

In this segment of material, noting that the field is uniform, from (1.1-7) we have that

$$F_{a,b} = lH \tag{1.3-3}$$

Solving for the field intensity,

$$H = \frac{F_{a,b}}{l} \tag{1.3-4}$$

Combining (1.3-2) with (1.3-4)

$$B = \frac{\mu}{l} F_{a,b} \tag{1.3-5}$$

Again noting that the field and flux density are uniform, the flux from node *a* to node *b* may be expressed

$$\Phi_a = \frac{A\mu}{l} F_{a,b} \tag{1.3-6}$$

which can also be written as

$$\Phi_a = P_{a,b} F_{a,b} \tag{1.3-7}$$

where the permeance $P_{a,b}$ is defined as

$$P_{a,b} = \frac{A\mu}{l} \tag{1.3-8}$$

Dividing (1.3-7) by the permeance yields Ohms' law for magnetic circuits,

$$F_{a,b} = R_{a,b} \Phi_a \tag{1.3-9}$$

where $R_{a,b}$ is the reluctance from node a to node b. From (1.3-8) and (1.3-9) this reluctance is given by

$$R_{a,b} = \frac{l}{A\mu} \tag{1.3-10}$$

The equivalent circuit element is depicted in Figure 1.3-2b.

### 1.3.2 Nonlinear Material

In Section 1.3-1, we considered Ohm's law in the context of a magnetically linear material. In practice, most magnetic materials are subject to both saturation and magnetic hysteresis. Under many cases, an adequate analysis of an electromechanical system can be made by considering only magnetic saturation. To illustrate this, let us again consider Fig. 1.3-2 subject to the same assumptions as Section 1.3-1 except that we allow magnetic saturation to occur. In this case, the relationship between flux density and field intensity becomes

$$\mathrm{B} = \mu_\theta(\theta)H \tag{1.3-11}$$

where $\theta$ can be either $B$ or $H$, depending upon how the permeability function is defined.

The relationships (1.3-3)-(1.3-6) are still valid except that the permeability is no longer a constant. Thus

$$\Phi_a = \frac{\mathrm{A}\mu_\theta(\theta)}{l} F_{a,b} \tag{1.3-12}$$

which may be expressed

$$\Phi_a = P(\xi)F_{a,b} \tag{1.3-13}$$

where

$$P(\xi) = \begin{cases} \dfrac{A}{l}\mu_H(F_{a,b}/l) & \text{Form 1}: \xi = F_{a,b}; \theta = H \\ \dfrac{A}{l}\mu_B(\Phi_a/A) & \text{Form 2}: \xi = \Phi_a; \theta = B \end{cases} \tag{1.3-14}$$

As can be seen, the permeance in (1.3-14) is either a function of the MMF drop across the element and hence the permeability is formulated as a function of the $H$ field, or the permeance is a function of flux density and the permeability is in turn expressed in terms of flux density.

Dividing by the permeance in (1.3-13) yields

$$F_{a,b} = R(\xi)\Phi_a \tag{1.3-15}$$

where

$$R(\xi) = \begin{cases} \dfrac{l}{A\mu_H(F_{a,b}/l)} & \text{Form 1}: \xi = F_{a,b}; \theta = H \\ \dfrac{l}{A\mu_{\mathbf{B}}(\Phi_a/A)} & \text{Form 2}: \xi = \Phi_a; \theta = B \end{cases} \tag{1.3-16}$$

### 1.3.3 PM Material

The $B$ versus $H$ characteristic for permanent magnet material is qualitatively the same as for other ferromagnetic and ferrite magnetic materials. The difference between permanent "hard" and non-permanent "soft" magnetic materials is the width of the hystereses loop. For this reason, the $B-H$ characteristic for the permanent magnet material shown in Fig. 1.3-3 is shown as being wider than the

permanent magnet material in Fig. 1.3-1. Another difference is that the practical use of the permanent magnet material is typically restricted to the normal operating range depicted in Figure 1.3-3. While it is possible to operate to the upper right in Figure 1.3-3, operating to the left of the indicated region causes permanent demagnetization.

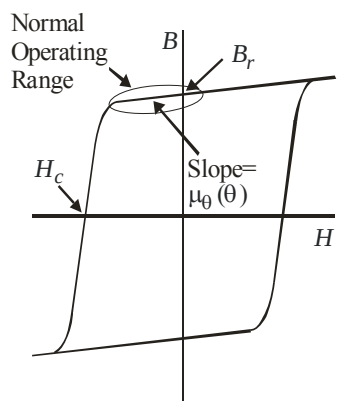


Figure 1.3-3. *B-H* characteristic of hard magnetic materials.

Because the region of operating point actually used is restricted (we normally do not traverse the entire curve), it is convenient to express the relationship between flux density $B$ and field intensity $H$ as

$$B = \mu_\theta(\theta)H + B_r \tag{1.3-20}$$

For a rectangular piece of material with length $l$ and cross sectional area $A$ it is readily shown that

$$\Phi_a = P(\xi)\, F_{a,b} + \Phi_r \tag{1.3-21}$$

where

$$\Phi_r = AB_r \tag{1.3-22}$$

and where

$$P(\xi) = \begin{cases} \dfrac{A}{l}\mu_H(F_{a,b}/l) & \text{Form1}: \xi = F_{a,b}; \theta = H \\ \dfrac{A}{l}\mu_B\big((\Phi_a - \Phi_r)/A\big) & \text{Form 2}: \xi = \Phi_a; \theta = B \end{cases} \tag{1.3-23}$$

Alternately, we may represent a section of permanent magnet material as

$$F_{a,b} = R(\xi)(\Phi_a - \Phi_r) \tag{1.3-24}$$

where

$$R(\xi) = \begin{cases} \dfrac{l}{A\mu_H(F_{a,b}/l)} & \text{Form 1}: \xi = F_{a,b}; \theta = H \\ \dfrac{l}{A\mu_B\big((\Phi_a - \Phi_r)/A\big)} & \text{Form 2}: \xi = \Phi_a; \theta = B \end{cases} \tag{1.3-25}$$

The resulting equivalent circuit is depicted in Figure 1.3-4.

Before concluding this section some final comments are in order. First, because the operating range normally used is restricted, $\mu_\theta$ can often be taken to be constant; it will generally be close to the permeability of free space, $\mu_0$. Second, it should be recognized that the parameters of the $B-H$ characteristic are highly temperature dependent, which makes some materials inappropriate for some applications.

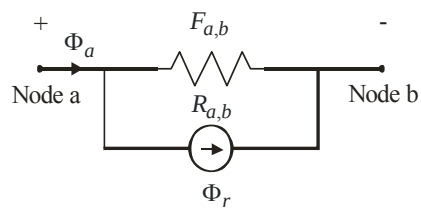


Figure 1.3-4. Equivalent magnetic circuit for permanent magnet material.

## 1.4 THE MEAN PATH APPROXIMATION AND CONSTRUCTION OF THE MAGNETIC EQUIVALENT CIRCUIT

In this section, the procedure whereby we translate a geometrical description of a device into a magnetic equivalent circuit is considered by way of a relatively simple example – a UI core inductor. The analysis presented herein is crude – it is certainly not sufficiently accurate to perform a design. However, it will be useful in illustrating the procedure for obtaining the magnetic equivalent circuit. It will also be useful in the next section wherein the translation of magnetic circuits to electric circuits is considered. Of course, the ultimate goal of this analysis is to provide an analysis which is of sufficient accuracy to facilitate design. To this end, a second and considerably more detailed example is set forth in Section 1.6.

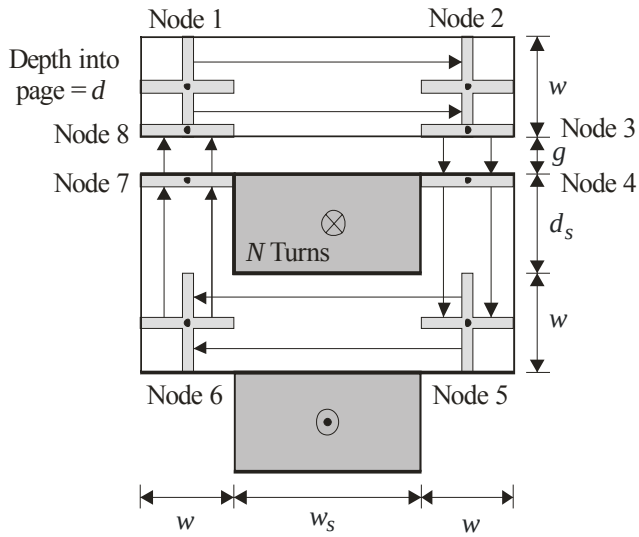


Figure 1.4-1. UI core inductor. Light shading indicates nodes. Dark shading indicates winding region.

## 1.4.1 A UI CORE INDUCTOR

Figure 1.4-1 illustrates a UI core inductor. It consists of a 'U' and 'I' shaped pieces of ferromagnetic (for a low-frequency inductor) or ferrimagnetic (for a high-frequency inductor) material separated by an air gap. All dimensions are indicated in the figure; note that the core extends a depth $d$ into the page. The dark region indicates the area where the windings are placed. Also indicated in the figure is the direction of the positive flux flow for positive current.

## 1.4.2 SELECTION OF NODES

The first step in the analysis is to select node locations for the magnetic equivalent circuit. In doing this, it is important to realize that there is no unique choice. In essence, the role of the nodes is to break the circuit into regions which may be treated as a simple reluctance; either linear or nonlinear. These nodes should have the property that there is negligible (preferably zero) MMF drop across them, because they will be treated as equipotential points in the equivalent circuits. In general, there is a tradeoff between accuracy and the number of nodes. Another factor in selecting nodes is that they usually mark the endpoints of regions that can be treated by simple, lumped, magnetic circuit elements.

One possible selection of nodes is illustrated in Figure 1.4-1. Therein, the nodes are number 1-8. The thickness of these nodes will be allowed to go to zero in the limit. Note that the cross sectional area of most of the nodes is a rectangle; however nodes 1,2,5, and 6 have a '+' shape; these are nodes in which the flux enters in one direction, and is assumed to make a right angle turn into another direction. Since flux does not make right angle turns, it is somewhat surprising that this technique will yield acceptable results; yet the author would like to assure the reader that this is in fact the case. The biggest error in Figure 1.4-1 is not the assumption of the flux magically making right angle turns in Figure 1.4-1; it is instead the fact that we have not accounted for fringing flux. This will be addressed in Section 1.6.

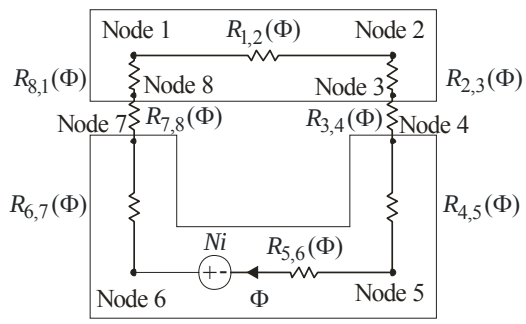


Figure 1.4-2. A magnetic equivalent circuit representing the UI core inductor.

## 1.4.3 THE MEAN PATH APPROXIMATION

The next step in developing the magnetic equivalent circuit is to connect the nodes with circuit elements representing the reluctance between nodes, and to represent the MMF sources. In connecting these nodes, we will often estimate the reluctance between nodes by representing the distance between nodes as a rectangular section of material (such as in Figure 1.3-2) wherein the length of the rectangular section is given by the mean distance between nodes. This procedure is known as the mean path approximation, and results in the equivalent circuit shown in Figure 1.4-2. Therein, the reluctance have been expressed as functions of the flux going through them, and so the permeability function has been taken to be a function of flux density. From geometrical constraints, we have that

$$R_{1,2}(\Phi) = R_{5,6}(\Phi) = \frac{w_s + w}{wd\mu_B(\Phi/(wd))} \tag{1.4-1}$$

$$R_{2,3}(\Phi) = R_{8,1}(\Phi) = \frac{w}{2wd\mu_B(\Phi/(wd))} \tag{1.4-2}$$

$$R_{3,4} = R_{7,8} = \frac{g}{wd\mu_0} \tag{1.4-3}$$

$$R_{4,5}(\Phi) = R_{6,7}(\Phi) = \frac{d_s + w/2}{wd\mu_B(\Phi/(wd))} \tag{1.4-4}$$

At this point, the nodes and majority of the circuit elements values associated with the U-I core example have been discussed. However, one important point remains, that is the MMF source in Figure 1.4-2. Treatment of the MMF sources will be considered in the following section.

## 1.4-4 MMF SOURCES

From Kirchoff's MMF law, the sum of the MMF drops around a closed loop is equal to the sum of the MMF sources for that loop. Thus, traversing the nodes in the order 1,2, … 7,8,1 in Figure 1.4-2, the sum of the voltage drops must be equal to the enclosed current which, by the right-hand rule, is $Ni$. Placing the current source as shown, we see that this requirement is satisfied, i.e.,

$$Ni = \left(R_{1,2}(\Phi) + R_{2,3}(\Phi) + \cdots R_{7,8}(\Phi) + R_{8,1}(\Phi)\right)\Phi \tag{1.4-5}$$

The placement in this example, and in many examples, is highly arbitrary since the MMF source could have been placed between any two nodes and (1.4-5) would be satisfied. However, some restrictions do apply; these arise because the MMF sources must satisfy Kirchoff's MMF law for all current loops. As an exercise, the reader should observe that had we traversed the loop in the opposite direction, i.e. 8,7, .. 2,1,8 then the enclosed current would have been $-Ni$. If we had assumed a positive direction for the flux to be in the opposite direction of the one chosen; the net effect of these two changes would be to flip the polarity of the MMF source. The numerical results obtained would be identical.

## 1.4-5 CIRCUIT REDUCTIONS

All network reduction techniques the reader is accustomed to for electric resistive circuits also apply to magnetic circuits. These network reduction include series combinations, parallel combinations, voltage division, and current division. This is because these techniques are all based on Kirchoff's law's which are basically identical for electric and magnetic circuits. The only caution that needs to be taken is when the reluctances are a nonlinear function of flux through the branch; in this case we need to develop appropriate expressions for the flux in each branch. In this U-I core example, we have a common flux through all reluctances. Hence, we can combine the series resistances to form the simple network shown in Figure 1.4-3. Therein,

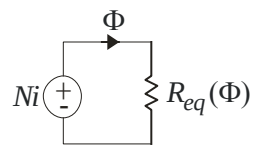


Figure 1.4-3. Simplified magnetic equivalent circuit for a UI core inductor.

$$R_{eq}(\Phi) = R_{1,2}(\Phi) + R_{2,3}(\Phi) + R_{3,4}(\Phi) + R_{4,5}(\Phi) + R_{5,6}(\Phi) + R_{6,7}(\Phi) + R_{7,8}(\Phi) + R_{8,1}(\Phi) \tag{1.4-5}$$

In summary, Figure 1.4-2 is the magnetic equivalent circuit for our U-I core. At this point, the reader is probably dissatisfied for two good reasons; first the equivalent circuit of Figure 1.4-2 is almost trivially simple – it does not provide a good example of network reductions, for example. Secondly the reader still has not been provided with a concrete example of the accuracy of the model. Finally, we have not discussed the translation of magnetic equivalent circuits to electric circuits. This latter point will be addressed in the next section; and the reader is promised a resolution of the first two issues in Section 1.6.

## 1.5 TRANSLATION OF MAGNETIC CIRCUITS TO ELECTRIC CIRCUITS

The magnetic equivalent circuit is a tool that we can use to relate flux $\Phi$ to a MMF source $Ni$. Often, however, it is our desire to develop an electrical circuit model that will represent an electromechanical device. In this section, we will consider the relationship between the magnetic equivalent circuit and the electric equivalent circuit.

### 1.5.1 Flux Linkage

The basic concept of flux as the integral of flux density over a finite surface was set forth in (1.2-3). The concept of flux linkage is closely related to the concept of flux. In particular, let us assume that a winding is wound around the periphery of a surface '$x$', and that the flux linking this surface is $\Phi_x$. Then, the flux linking this winding is denoted $\lambda_x$ and is related to the flux by

$$\lambda_x = N_x \Phi_x \tag{1.5-1}$$

where $N_x$ is the number of turns. It should be observed that for this to be true the direction of the winding, that is the defined direction for positive current, must be counterclockwise around the surface as viewed from a vantage wherein the defined

direction of positive flux is toward the observer. Alternately, stated in terms of the 'right hand rule,' if the fingers of one's right hand wrap around the periphery of a surface in the defined direction for positive current, then one's right thumb (extended away from one's hand) will be pointing in the defined direction for positive flux. If this convention is not followed, then a '-' sign is introduced into (1.5-1).

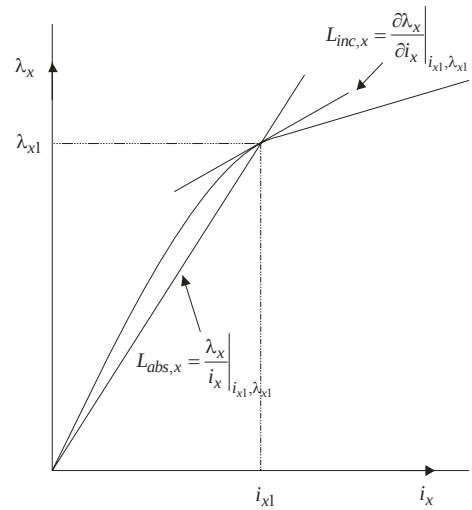


Figure 1.5-1. Flux linkage versus current.

### 1.5.2 Inductance

Let us consider a system with a single winding 'x'. Neglecting hysteresis, the relationship between flux linkage through winding 'x' and the current into winding 'x' is depicted in Figure 1.5-1. We will use this figure to introduce the concept of inductance. In particular, the absolute inductance at an operating point $i_{x1,}\lambda_{x1}$ is defined as

$$L_{abs,x} = \left.\frac{\lambda_x}{i_x}\right|_{i_{x1},\lambda_{x1}} \tag{1.5-2}$$

Also of interest is the incremental inductance, which is defined as the slope of the flux linkage versus current characteristic at a given operating point. In particular

$$L_{inc,x} = \left.\frac{\partial \lambda_x}{\partial i_x}\right|_{i_{x1},\lambda_{x1}} \tag{1.5-3}$$

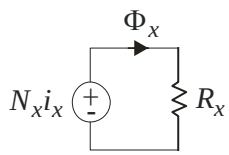


Figure 1.5-2. Simplified magnetic equivalent circuit for a UI core inductor.

Several observations are in order. First, the incremental inductance is generally lower than the absolute inductance. Secondly, in a magnetically linear system, the absolute and incremental inductances are the same. Finally, it should be noted that the '*abs*' or '*inc*' subscripts are normally not used; these will have to be ascertained from the context of the discussion.

In order to understand how inductance is related to our MEC, consider the simple magnetic equivalent circuit shown in Figure 1.5-2. Therein flux in winding 'x' would be proportional to the MMF as

$$\Phi_x = \frac{N_x i_x}{R_x} \tag{1.5-4}$$

From (1.5-1)

$$\lambda_x = \frac{N_x^2 i_x}{R_x} \tag{1.5-5}$$

Thus

$$\frac{\lambda_x}{i_x} = L_x = \frac{N_x^2}{R_x} \tag{1.5-6}$$

Since $R_x$ is constant, this system is magnetically linear and there is no reason to distinguish between absolute and incremental inductance.

In a magnetic system with a single winding, the inductance is a self inductance. In other words, the inductance relates how much flux links a winding due to the amount of current in that winding. In systems with multiple windings, self inductance is still of interest. However, in addition, there is also the concept of mutual inductance which relates how much flux will appear in a given winding to a current in a different winding.

Let us consider a system with several windings. In linear magnetic systems, or when discussing incremental inductance, the mutual inductance $L_{x,y}$ between winding '$x$' and winding '$y$' describes how much the flux linking winding '$x$' changes due to a change in the current in winding '$y$'. In particular,

$$L_{x,y} = \frac{\partial \lambda_x}{\partial i_y} \tag{1.5-7}$$

Ordinarily, the concept of absolute self and mutual inductances is not terribly useful in multi-winding nonlinear magnetic systems. Instead, it is more common to define flux linkages in terms of a leakage component and magnetizing component; and then relate the magnetizing flux to a magnetizing current in a way where it can essentially be treated as a single-winding problem.

### 1.5.3 Faraday's Law

Consider a winding '$x$' on an electromechanical device. Denoting the voltage across the winding as $v_x$, Faraday's law states the voltage across the winding is equal to the time rate of change of the flux linkages. If we allow for an Ohmic drop $r_x i_x$ where $r_x$ is the resistance of the winding, we thus have that

$$v_x = r_x i_x + \frac{d\lambda_x}{dt} \tag{1.5-8}$$

Equation (1.5-8) is extremely important; it will form the basic voltage equation for nearly every device considered throughout this work.

Before concluding this section, let us briefly return to the system shown in Figure 1.5-2. From (1.5-6), we have that

$$\lambda_x = L_x i_x \tag{1.5-9}$$

Substitution of (1.5-9) into (1.5-8) yields

$$v_x = r_x i_x + L_x \frac{di_x}{dt} \tag{1.5-10}$$

Note that this simple form is only possible if $L_x$ is constant; otherwise there will be additional terms.

Before concluding this discussion, let us briefly consider the energy stored in an inductor. The electrical power flowing into the winding is given by

$$p_x = v_x i_x \tag{1.5-11}$$

Upon ignoring losses (i.e. setting $r_x = 0$), (1.5-10) and (1.5-11) yield

$$p_x = L_x i_x \frac{di_x}{dt} \tag{1.5-12}$$

Let us suppose that at time $t = 0$ the inductor current, and stored energy, are zero. Let us further suppose that at time $t = t_1$, the inductor current is $i_x = i_{x1}$. The energy flowing into the inductor (and hence stored in the inductor) may be expressed

$$E_x = \int_{t=0}^{t_1} p_x dt \tag{1.5-13}$$

Substitution of (1.5-12) into (1.5-13) yields

$$E_x = \int_{i_x=0}^{i_x=i_{x1}} L_x i_x di_x \tag{1.5-14}$$

which reduces to

$$E_x = \frac{1}{2} L_x i_{x1}^2 \tag{1.5-15}$$

Since this expression is valid for any value of $i_{x1}$, we may more simply write the familiar expression

$$E_x = \frac{1}{2} L_x i_x^2 \tag{1.5-16}$$

This well known result will prove valuable in the next section when we wish to calculate leakage inductance.

## 1.6 ANALYSIS OF AN EI CORE INDUCTOR

In this section, we will consider the detailed analysis of an EI core inductor using magnetic equivalent circuit modeling. Our objective will be to start with a geometrical description of a core and its material properties, and end with an electrical description in terms of the $\lambda - i$ characteristic of the device.

### 1.6.1 EI Core MEC Structure

Figure 1.6-1 illustrates the EI core arrangement. An initial list of parameters of includes:

| | |
|---|---|
| $w_i$ | width of the I portion of the core |
| $g$ | airgap between E and I sections of the core |
| $d_s$ | slot depth |
| $w_s$ | slot width |
| $d_w$ | winding depth |
| $w_w$ | width of the winding |

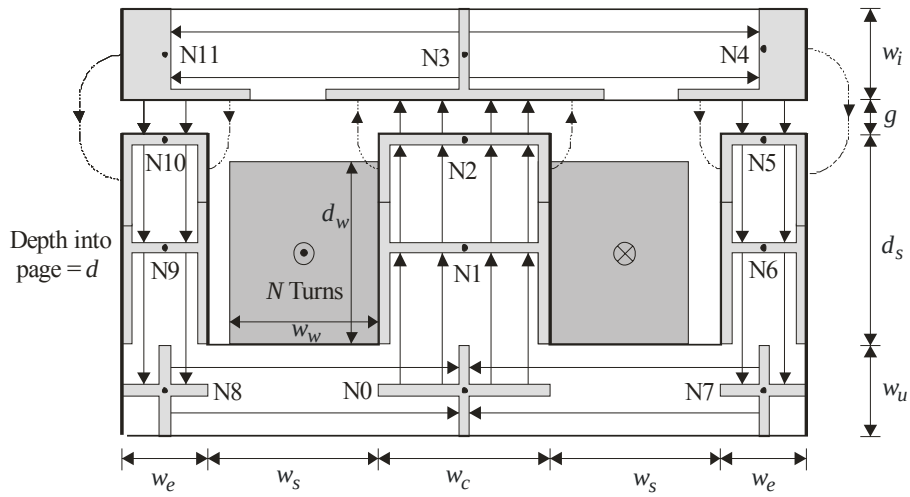


Figure 1.6-1. Inductor geometry and node positions.

| | |
|---|---|
| $w_e$ | width of the end post of the E core |
| $w_c$ | width of the center post of the E core |
| $w_u$ | width of the underside of the E core |
| $d$ | depth into page |
| $N$ | number of turns |

The reader will notice that the node shapes are considerably different than those considered in the case of the UI core inductor. For the most part, this is not because of the difference of arrangement; rather, it is because in this case we will pursue a model which is accurate enough for design purposes. As a result, we will need to consider the fringing flux paths shown in Figure 1.6-1, and consider additional nodes in the circuit. In addition to the ones shown, we will also consider fringing flux paths extending in front of and behind the cores, as well as a path for a leakage flux.

The MEC for any physical arrangement is not unique. Herein, we will consider the MEC depicted in Figure 1.6-2. Observe that in this case, we have elected to label the diagram in terms of permeances rather than reluctances. Based on our earlier discussion, and Figure 1.6-1, the reader will see where the permeance terms of the form $P_{x,y}$ arise, where '$x$' and '$y$' denote node numbers. However there are a number of additional terms included in Figure 1.6-2. In particular, $P_{vl}$, $P_{vb}$, $P_{hl}$, $P_{hb}$, $P_f$ denote vertical slot leakage permeance, vertical bypass permeance, horizontal leakage permeance, horizontal bypass permeance, and face permeance respectively.

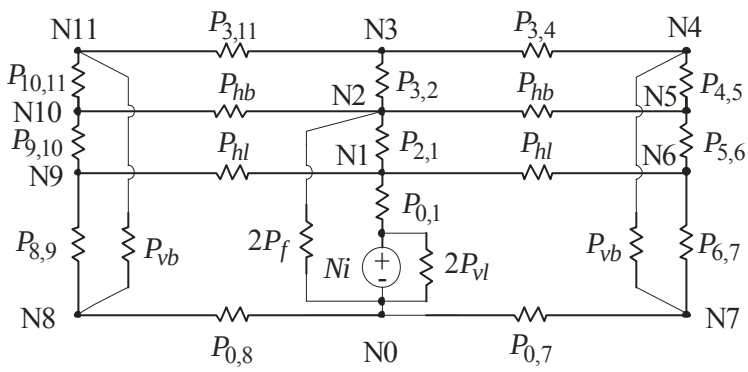


Figure 1.6-2. EI core inductor MEC.

### 1.6.2 Core Permeances

We begin our analysis by considering the permeances corresponding to magnetic paths in the magnetic material. In particular, we have

$$P_{0,1} = \frac{2dw_c}{d_s + w_u}\mu(\bullet) \tag{1.6-1}$$

$$P_{1,2} = \frac{2dw_c}{d_s}\mu(\bullet) \tag{1.6-2}$$

$$P_{3,4} = \frac{2dw_i}{2w_s + w_e + w_c}\mu(\bullet) \tag{1.6-3}$$

$$P_{5,6} = P_{9,10} = \frac{2dw_e}{d_s}\mu(\bullet) \tag{1.6-4}$$

$$P_{6,7} = P_{8,9} = \frac{2dw_e}{d_s + w_u}\mu(\bullet) \tag{1.6-5}$$

$$P_{0,7} = P_{0,8} = \frac{2dw_u}{w_c + w_e + 2w_s}\mu(\bullet) \tag{1.6-6}$$

In each case, the permeances are a function of the permeability which may be formulated either as a function of the flux density or field intensity in the material of interest.

### 1.6.3 Air Gap Permeances

Our next step will be to calculate the air gap reluctances $P_{2,3}$, $P_{4,5}$, and $P_{10,11}$. At first thought, we may be tempted to express these reluctances as

$$P_{2,3} = \frac{w_c d \mu_0}{g} \tag{1.6-7}$$

and

$$P_{4,5} = P_{10,11} = \frac{w_e d \mu_0}{g} \tag{1.6-8}$$

However, such an approach will typically not be sufficiently accurate for design purposes. This is due to the fringing flux indicated by dotted lines in Figure 1.6-1. In addition to the paths indicated, fringing flux will also be present in front of and behind the core sections. The effect of the fringing flux will be to significantly increase the airgap permeance.

In order to incorporate fringing flux into our analysis, let us first consider the fringing flux between the two indicated nodes in Figure 1.6-3. Therein, we will assume that the flux starts at the upper node, follows a semi-circular path until the gap; proceed directly down in the region of the gap, and then follows the semi-circular path to the bottom node. Clearly, the field lines will not follow such a convenient path. However, flux does tend to transition between magnetic materials and air in a normal fashion; and it will have the indicated direction at the center of the path; thus, at least at the endpoints and the center the path is correct. From basic geometrical arguments, the length of this path at a position $r$ is

$$l(r) = \pi r + g_p \tag{1.6-8}$$

Since the nodes are equipotential surfaces, the MMF drop between the two nodes is constant. Therefore the flux density along the indicated path may be expressed

$$B(r) = \mu_0 \frac{F}{\pi r + g_p} \tag{1.6-10}$$

where $F$ is the MMF drop between the two nodes. The total flux flowing between the two nodes may be expressed

$$\Phi = \int_0^{h_p} B(r) d_p dr \tag{1.6-11}$$

Substitution of (1.6-10) into (1.6-11) yields

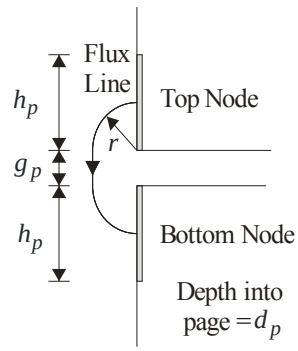

Figure 1.6-3. Fringing flux geometry.

$$\Phi = F\frac{\mu_0 d_p}{\pi}\ln\left(1+\frac{\pi h_p}{g_p}\right) \tag{1.6-12}$$

so the permeance of the indicated flux path becomes

$$P = \frac{\Phi}{F} = \frac{\mu_0 d_p}{\pi}\ln\left(1+\frac{\pi h_p}{g_p}\right) \tag{1.6-13}$$

Using an identical technique for the geometry for Figure 1.6-4 we have that for this situation

$$P = \frac{\Phi}{F} = \frac{2\mu_0 d_p}{\pi}\ln\left(1+\frac{\pi h_p}{2g_p}\right) \tag{1.6-14}$$

At this point, we have the tools we need to calculate the air gap reluctances including the fringing flux terms. In particular, we can formulate $P_{2,3}$ as

$$P_{2,3} = P_d + P_{fl} + P_{fr} + P_{ff} + P_{fb} \tag{1.6-15}$$

where $P_d$ is the permeance of the path directly across the airgap, and $P_{fl}$, $P_{fr}$, $P_{ff}$, and $P_{fb}$ denote the permeance of the fringing flux paths to the left of, to the right of, to the front of, and to the back of the direct path.

The permeance of the direct path may be readily expressed

$$P_d = \frac{\mu_0 w_c d}{g} \tag{1.6-16}$$

Applying (1.6-14) to the geometry of Figure 1.6-1,

$$P_{fl} = P_{fr} = \frac{2\mu_0 d}{\pi}\ln\left(1+\frac{\pi\min(w_s/2, d_s/2)}{2g}\right) \tag{1.6-17}$$

In (1.6-17) it can be seen that $h_p$ of (1.6-14) was taken to be the minimum of $w_s/2$ or $d_s/2$. Actually, the selection of these limits is not critical since (1.6-14)

increases rather slowly with $h_p$. In this case, the choice was made by dividing the slot area into rectangular regions – one associated with fringing flux in each corner. Next the largest semi-circle that could be placed in the upper corners was used as a basis to select $h_p$. With this line of reasoning, the reader may question why fringing flux wasn't included in bottom corners of Figure 1.6-1. Actually, it will exist; however, since there is no airgap the term is not as significant.

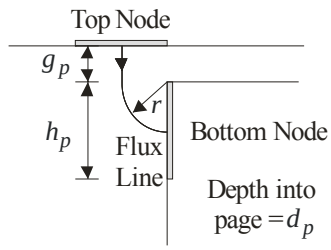


Figure 1.6-4. Another fringing flux geometry.

Next, we turn our attention to $P_{ff}$ and $P_{fb}$. Utilizing (1.6-13) with $d_p = w_c$ (because of the orientation) and with $h_p = w_i$, we have that

$$P_{ff} = P_{fb} = \frac{\mu_0 w_c}{\pi} \ln\left(1 + \frac{\pi w_i}{g}\right) \tag{1.6-18}$$

Substitution of (1.6-16-(1.6-18) into (1.6-15) yields

$$P_{2,3} = \frac{\mu_0 w_c d}{g} + \frac{4\mu_0 d}{\pi} \ln\left(1 + \frac{\pi \min(w_s/2, d_s/2)}{2g}\right) + \frac{2\mu_0 w_c}{\pi} \ln\left(1 + \frac{\pi w_i}{g}\right) \tag{1.6-19}$$

Following a very similar procedure for $P_{4,5}$ and $P_{7,8}$ we arrive at

$$P_{4,5} = P_{10,11} = \frac{\mu_0 w_e d}{g} + \frac{\mu_0 (d + 2w_e)}{\pi} \ln\left(1 + \frac{\pi w_i}{g}\right) + \frac{2\mu_0 d}{\pi} \ln\left(1 + \frac{\pi \min(w_s/2, d_s/2)}{2g}\right) \tag{1.6-20}$$

### 1.6.4 Horizontal Permeances

The next permeance elements we will consider are the horizontal leakage and bypass permeances, $P_{hl}$ and $P_{hb}$. These permeances both result from a horizontal flux component in the slot. We will first consider the horizontal leakage permeance which corresponds to flux paths 1 and 2 in Figure 1.6-5. Path 3 will be discussed in the context of the horizontal permeances. Observe that $x$ will be used

in a variety of derivations corresponding to the three paths – we will only be considering one at a time. Further, note that these paths apply to either slot; they are shown in both slots only to result in a cleaner diagram.

Let us consider the hypothesis that there will be a component of flux following path 1 in the lower part of the figure. The reader may be surprised that this path is considered leakage since it makes use of the magnetic material. This is not really unusual – leakage flux often makes use of a certain amount of magnetic material (this is why leakage inductances can be susceptible to saturation). The salient feature, however, is that it doesn't follow the primary magnetizing path. Also, note that flux following this path does not link the entire winding.

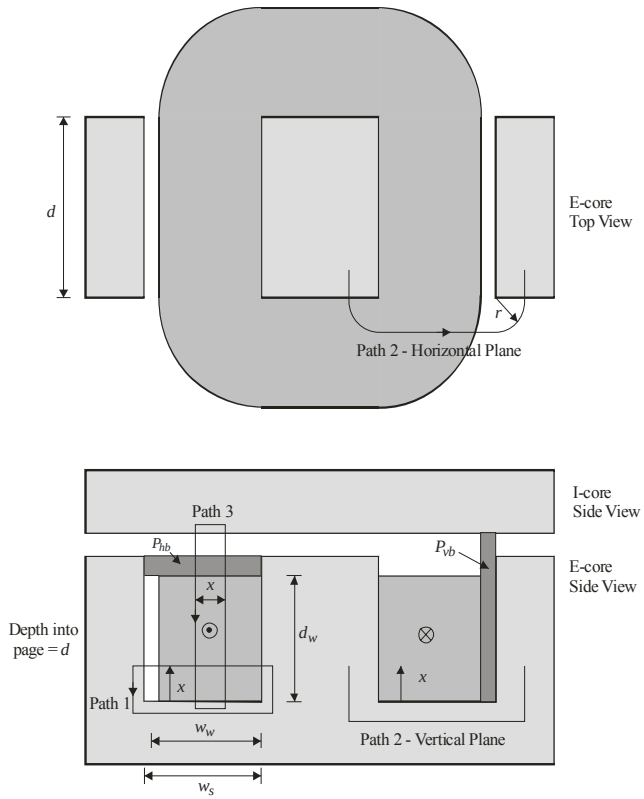


Figure 1.6-5. Calculation of leakage flux through slot.

The amount of current enclosed by path 1 may be expressed

$$i_{enc} = \frac{xNi}{d_w} \tag{1.6-21}$$

Assuming that the field intensity is uniform within the slot, and may be neglected in the magnetic material, from Ampere's law we have that

$$Hw_s = i_{enc} \tag{1.6-22}$$

Substitution of (1.6-21) into (1.6-22)

$$H = \frac{xNi}{d_w w_s} \tag{1.6-23}$$

The magnetic energy stored in a region of space may be expressed [2]

$$E = \frac{1}{2}\int_v \mathbf{B}\cdot\mathbf{H}dv \tag{1.6-24}$$

where $v$ denotes a volume. In the non-magnetic winding, in which $\mathbf{B} = \mu_0\mathbf{H}$, we have that

$$E = \frac{1}{2}\mu_0\int_v |\mathbf{H}|^2 dv \tag{1.6-25}$$

For the problem at hand, we will integrate over the slot volume in the region $x < d_w$. The reader may question why we don't extend the volume to the entire slot. We will do so at the end of this section; for this is the source of the horizontal bypass permeance.

Taking our differential volume element to be

$$dv = dw_s dx \tag{1.6-26}$$

Substitution of (1.6-23) and (1.6-26) into (1.6-25) yields

$$E = \frac{1}{2}\mu_0\int_{x=0}^{d_w}\left(\frac{xNi}{d_w w_s}\right)^2 dw_s dx \tag{1.6-27}$$

Evaluating (1.6-27) yields

$$E = \frac{\mu_0 N^2 i^2 d_w d}{6w_s} \tag{1.6-28}$$

From (1.6-28), we are finally in a position to compute the leakage reluctance. Recall from (1.5-12) that the energy stored in a linear leakage inductance $L_l$ may be expressed

$$E = \frac{1}{2} L_l i^2 \tag{1.6-29}$$

and, from (1.5-6), a linear (leakage) inductance can be expressed in terms of a (leakage) reluctance as

$$L = N^2 P \tag{1.6-30}$$

Combining (1.6-29) and (1.6-30) we have that the horizontal leakage permeance due to path 1 may be expressed

$$P_{hl,p1} = \frac{2E}{N^2 i^2} \tag{1.6-31}$$

Substitution of (1.6-28) into (1.6-31) yields the permeance associated with path 1:

$$P_{hl,p1} = \frac{\mu_0 d_w d}{3 w_s} \tag{1.6-32}$$

As it turns out that while (1.6-32) is the dominant contribution to the horizontal leakage flux, there is another term associated with the end turns of the winding. This second term corresponds to path 2 in Figure 1.6-5, and is a result of flux in front of and behind the slot.

Let us consider path 2 in detail. This is a three dimensional path, with both horizontal and vertical components. However, temporarily assuming that the magnetic material in infinitely permeable, only the horizontal portion of the path is relevant to our analysis; and of that only the portion that is not in the magnetic material is relevant – in other words we are only interested in the portion of the path in air.

The current enclosed by path 2 is given by (1.6-21). Using the techniques that we have already established we can find the H field for a path at radius $r$ and height $x$. In particular, we have that

$$H = \frac{xNi}{d_w (w_s + \pi r)} \tag{1.6-33}$$

Using the energy technique just illustrated, based on $0 \le x \le d_w$ and $0 \le r \le \min(w_e, w_c / 2)$ we have that the permeance associated with path 2 may be expressed

$$P_{hp,p2} = \frac{2d_w\mu_0}{3\pi}\ln\left(1+\frac{\pi\min(w_e, w_c/2)}{w_s}\right) \tag{1.6-34}$$

The total leakage reluctance can than be calculated as the parallel combination of the two reluctances, i.e.

$$P_{hl} = P_{hl,p1} + P_{hl,p2} \tag{1.6-35}$$

Given the location of the corresponding leakage flux, the horizontal leakage permeance is placed in a position corresponding to half-way up the slot, as depicted in Fig. 1.6-2.

As the reader has read this development, it may have been troublesome that the same paths for $d_w \le x \le d_s$ was not considered. This region corresponds to the dark rectangular shaded area in Fig. 1.6-5 labeled $P_{hb}$. Combining the permeance within the slot with the fringing terms in front of and behind the slot yields

$$P_{hb} = \frac{\mu_0 d(d_s - d_w)}{w_s} + \frac{2\mu_0(d_s - d_w)}{\pi}\ln\left(1+\pi\frac{\min(w_e, w_c/2)}{w_s}\right) \tag{1.6-36}$$

This permeance is placed towards the top of the core in light of where it is physically flowing. The derivation of (1.6-36) is left as a exercise for the reader; since $i_{enc}$ does not vary with $x$ the derivation is considerably simpler than $P_{hl}$.

### 1.6.4 Vertical Permeances

We will begin our discussion of the vertical permeances with the vertical slot leakage permeance $P_{vsl}$. To calculate this permeance, consider path 3 in Fig. 1.6-5. Observe that the current enclosed by the path is

$$i_{enc} = Ni\frac{2x}{w_w} \tag{1.6-37}$$

whereupon the vertical component field intensity in the direction of the path may be expressed

$$H = \frac{Nix}{w_w(d_s + g)} \tag{1.6-38}$$

Using the same energy methods as used previously, we obtain

$$P_{vl} = \frac{1}{12}\frac{\mu_0 d w_w}{d_s + g} \tag{1.6-39}$$

The reader may notice that the fringing vertical flux in front of and behind the slot in the paths has not been accounted for in the calculation of the vertical leakage permeance. This is because the vertical terms are much less significant than the corresponding horizontal terms. As a result, the additional effort is not warranted.

Next, we turn our attention to the vertical bypass permeance. This corresponds the permeance path between the winding and the far edge of the core, illustrated by dark shading in Figure 1.6-5. The permeance of the straight segment plus fringing flux in front and back

$$P_{vb} = \frac{\mu_0 d(w_s - w_w)}{d_s + g} + \frac{2}{\pi}\mu_0 (w_s - w_w)\ln\left(1 + \pi\frac{\min(w_i, w_u)}{d_s + g}\right) \tag{1.6-40}$$

If the winding is narrow compared to the slot, then (1.6-40) will dominate (1.6-39); this is why the fringing flux has been included.

### 1.6.5 Face Permeance

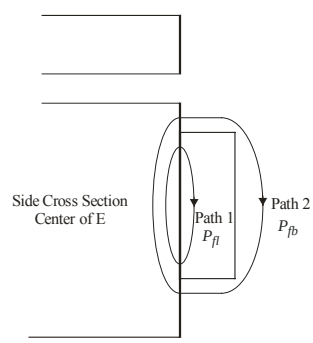


Figure 1.6-6. Face permeances.

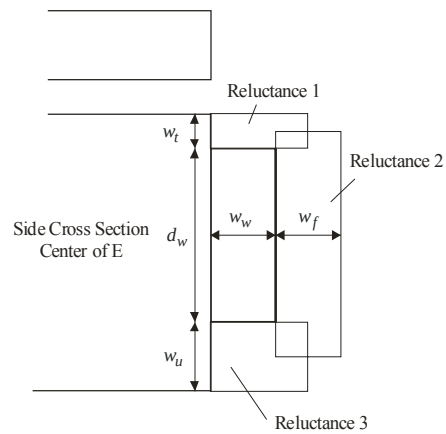

Figure 1.6-7. Face bypass permeance.

$$w_t = d_s - d_w$$

$$P_f = P_{fl} + P_{fb}$$

$$R_{fb} = \frac{2w_w + w_f}{2\mu_0 w_c w_t} + \frac{2d_w + w_t + w_u}{2\mu_0 w_c w_f} + \frac{2w_w + w_f}{2\mu_0 w_c w_u}$$

$$w_f = \sqrt{\frac{(2d_w + w_t + w_u)w_t w_u}{w_t + w_u}}$$

$$R_{fb} = \frac{w_t + w_u}{\mu_0 w_t w_u w_c}\left( w_w + \sqrt{\frac{(2d_w + w_t + w_u)(w_u + w_t)}{w_u w_t}} \right)$$

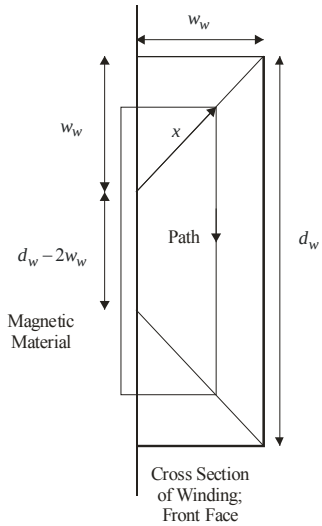

Figure 1.6-8. Face leakage permeance.

$$p = 2\sqrt{2}x + \left|d_w - 2w_w\right|$$

$$a = x^2 + \frac{x}{\sqrt{2}}\left|d_w - 2w_w\right|$$

$$i_{enc} = N\,i\,\frac{a}{w_w d_w}$$

$$Hp = i_{enc}$$

$$H = \frac{N\,i}{w_w d_w}\frac{a}{p}$$

$$E = \frac{1}{2}\int_{x=0}^{x_{max}} \underbrace{\mu_0 H^2}_{BH}\,\underbrace{w_c\,p\,\frac{dx}{\sqrt{2}}}_{dv}$$

$$x_{max} = \sqrt{2}\,\max(w_w, d_w/2)$$

$$E = \frac{\mu_0 N^2 i^2 w_c}{2\sqrt{2}d_w^2 w_w^2}\int_0^{x_{max}} \frac{a^2}{p}\,dx$$

$$P_{fl} = \frac{\mu_0 w_c}{16 w_w^2 d_w^2}\left[\begin{array}{l} x_{max}^4 + \sqrt{2}Kx_{max}^3 + \frac{1}{4}x_{max}^2 K^2 \\ -\frac{\sqrt{2}}{8}K^3 x_{max} + \frac{K^4}{16}\ln\left(1 + \frac{2\sqrt{2}x_{max}}{K}\right) \end{array}\right]$$

### 1.6.6 Simplified MEC and Circuit Solution

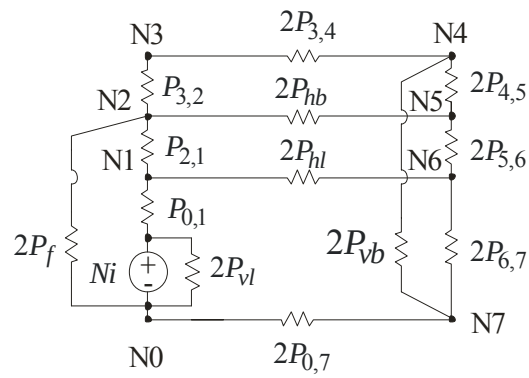


Figure 1.6-9. Simplified MEC.

### 1.6.7 EI Core Voltage Equation and Winding Resistance

Although the prediction of the $\lambda - i$ characteristic is critical to the electrical model, we must also consider the voltage equation which involves a winding resistance. From (1.5-8), the voltage equation for our system will be

$$v = ri + \frac{d\lambda}{dt} \tag{1.6-42}$$

However, we do not know the resistance. To estimate the resistance, using basic geometry it can be shown that the volume of the winding is

$$V_w = d_w w_w (2d + 2w_c + \pi w_w) \tag{1.6-43}$$

The conductor will only occupy a fraction of this volume since not all the space can be utilized. The ratio of the conductor volume to physical volume is known as the packing factor $p_f$. Thus the conductor volume may be expressed

$$V_c = V_w p_f \tag{1.6-44}$$

The cross sectional area of the conductor must be equal to the cross sectional area of the winding (times the packing factor), divided by the number of turns

$$A_c = \frac{w_w d_w p_f}{N} \tag{1.6-45}$$

Next, the cross sectional area of the conductor times the length of the conductor must be equal to the conductor volume. Thus,

$$L_c = \frac{V_c}{A_c} \tag{1.6-46}$$

Finally, resistance of the conductor may be expressed

$$r = \frac{L_c}{A_c \sigma_c} \tag{1.6-47}$$

where $\sigma_c$ is the conductivity of the conductor. Combining (1.6-41)-(1.6-46)

$$r = \frac{N^2 (2d + 2w_c + \pi w_w)}{\sigma_c p_f d_w w_w} \tag{1.6-48}$$

At this point, we know both how to calculate the flux linkage versus current characteristic for the flux linkage equation, and the resistance associated with the voltage equation. This is sufficient information to be able to calculate the electrical performance. In the next section, we will attempt this feat for a numerical example and compare our predictions to laboratory measurements.

### 1.6.8 EI Core Numerical Example

In order to conclude this work, we will consider a brief numerical example of the flux-linkage versus current relationship for an EI core inductor, and then compare the measured results to those predicted using the methods described in this chapter.

The geometrical parameters of the EI core used in the example are listed in Table 1.6-1. Physically, the core was created by stacking several U and I- cores to achieve the desired geometry.

Table 1.6-1. EI inductor dimensions in millimeters.

| | | |
|---|---|---|
| $d_s = 48.0$ | $d_w = 44.6$ | $w_i = 27.5$ |
| $w_s = 36.2$ | $w_w = 19.5$ | $w_e = 28.0$ |
| $w_u = 28.0$ | $w_c = 56.0$ | $d = 120$ |
| | $g = 3.05$ | |

The inductor winding was constructed using 40 turns of AWG #8 square wire, which has a cross sectional area of $8.37 \cdot 10^{-6}\ m^2$. Comparing this to the listed values of $w_w$ and $d_w$ yields a packing factor $p_f$ of 0.384, indicating a rather loose winding.

The magnetic material used was grade 3C85 ferrite. Data points taken from the manufacturers BH characteristic are listed in Table 1.6-2, so that the interested reader may reproduce these results. Therein field intensity is in A/m; flux density is in T.

Table 1.6-2. B-H data points.

| | | | | | | | | |
|---|---|---|---|---|---|---|---|---|
| *H* | 6.250 | 12.50 | 18.75 | 25.00 | 31.25 | 37.50 | 43.75 | 50.00 |
| *B* | 0.0917 | 0.150 | 0.190 | 0.215 | 0.250 | 0.273 | 0.292 | 0.318 |
| *H* | 56.25 | 62.50 | 68.75 | 75.00 | 81.25 | 87.50 | 93.75 | 100.0 |
| *B* | 0.383 | 0.350 | 0.360 | 0.370 | 0.375 | 0.382 | 0.388 | 0.392 |
| *H* | 150.0 | 175.0 | 200.0 | 225.0 | 250.0 | 275.0 | | |
| *B* | 0.408 | 0.416 | 0.423 | 0.428 | 0.430 | 0.432 | | |

The BH data of Table 1.6-2 was used to compute a function to represent permeability as a function of flux density. To this end, the permeability was assumed to be of the form:

$$\mu(B) = \mu_0 \frac{\frac{1}{K}\sum_{k=1}^{K} \sqrt[n_k]{(B/m_k)^{n_k} + (a_i)^{n_k}}}{\frac{1}{K}\sum_{k=1}^{K} \sqrt[n_k]{(B/m_k)^{n_k} + (a_i)^{n_k}} - 1} \tag{1.6-49}$$

where

$$a_i = \frac{\mu_{r,i}}{\mu_{r,i} - 1} \tag{1.6-50}$$

Setting $K = 1$ in (1.6-49) yields a functional form wherein the incremental permeability is $\mu_{r,1}\mu_0$ at $B = 0$ and $\mu_0$ at $B = \infty$. The use of $K > 1$ introduces a

greater number of degrees of freedom to help provide a more accurate fit to the data points.

Using curve-fitting techniques, the parameter vectors were determined to be

$$\mu_r = \begin{bmatrix} 8618 & 5105 \end{bmatrix} \tag{1.6-51}$$

$$n = \begin{bmatrix} 9.095 & 3.591 \end{bmatrix} \tag{1.6-52}$$

$$m = \begin{bmatrix} 0.7374 & 0.4856 \end{bmatrix} \tag{1.6-53}$$

The procedure to measure the flux-linkage versus current characteristics was as follows. First a 60 Hz sinusoidal source was applied to the machine winding and the applied voltage and current waveform were recorded. In addition, the voltage across a test coil located on the I-core at a point in the center of a slot was also recorded. The flux-linkage was determined by integrating

$$p\lambda = v - ri \tag{1.6-54}$$

This procedure is not as straightforward as it might seem; voltage and current offsets must be removed, and the value of resistance used must correspond to the ac resistance at that frequency (incorrect values of resistance cause widened hysteresis loops if the resistance is set to low, or inappropriate shapes if the value is set to high). The magnetizing flux linkage is found by integrating the voltage across the test coil, which only links magnetizing flux. In this case, it is still necessary to remove offsets, but it is unnecessary to subtract off a resistive term since there is no current flowing in the test winding.

At this point, the problem has been completely specified, and we may proceed to conduct our analysis. The results of this analysis are depicted in Figure 1.6-8. Therein, the measured and predicted total flux linkage versus current characteristics are shown. Also shown is the measured and predicted magnetizing flux linkage versus current characteristics. As can be seen, the MEC model predictions is reasonably consistent with the measured characteristics, although the hysteresis in the measured characteristics is significant.

As a final note, we will consider the computation of the winding resistance. Using (1.6-48), we obtain a value of 34 $m\Omega$. The measured value, obtained from a 4-wire digital multimeter, is 32 $m\Omega$. Again, the predicted results are reasonable close to the measured parameters.

## 1.7 ACKNOWLEDGEMENTS

The author of this chapter would like to gratefully acknowledge the support of ONR under the effort "National Naval Responsibility for Naval Engineering: Education and Research for the Electric Naval Engineer", Grant N00014-02-1-0623, without which this document would not have been possible. In addition, the author would like to express his gratitude to Jim Cale for designing, assembling, and collecting data for the EI inductor example in Section 1.6-6.

## 1.8 REFERENCES


[1] J.K. Watson, *Applications of Magnetism*, 2nd edition as published by author (1st edition published by John Wiley & Sons, Inc. 1980), 1985.

[2] W. H. Hayt, Jr., *Engineering Electromagnetics*, McGraw-Hill Book Company, 1981.

[3] D.C. Jiles and D.L. Atherton, "Ferromagnetic hysteresis," *IEEE Transactions on Magnetics*, vol. 19, no. 5, pp. 2183-2185, Sept 1983.

[4] K.H. Carpenter and S. Warren, "A wide bandwidth, dynamic hysteressis model for magnetization in soft ferrites," *IEEE Transactions on Magnetics*, vol. 28, no. 5, pp. 2037-2041, Sept 1992.

[5] D. Jiles, *Introduction to Magnetism and Magnetic Materials*, 2nd ed. London: Chapman & Hall, 1998.

[6] F. Preisach, "Über die magnetische Nachwirkung," *Zeitschrift für Physik*, vol. 94, pp. 277-302, Mar./May 1935.

[7] B.S. Guru, H.R. Hiziroğlu, Electric Machinery and Transformers, 2nd ed. , Harcourt Brace & Company, 1995.


## 1.9 AUTHOR'S NOTES (TO HIMSELF).

Think about some problems.